



# Image Description using Radial Associated Laguerre Moments

Bojun Pan<sup>1</sup>, Yihong Li<sup>2</sup> & Hongqing Zhu<sup>3\*</sup>

<sup>1</sup>College of Engineering, Northeastern University,  
Boston, Massachusetts 02115, USA

<sup>2</sup>Technology Center, AVIC Shaanxi Baocheng Aviation Instrument Co., Ltd,  
Baoji, Shaanxi 721006, China

<sup>3</sup>School of Information Science & Engineering,  
East China University of Science and Technology, Shanghai 200237, China  
Email: pan.bo@husky.neu.edu

**Abstract.** This study proposes a new set of moment functions for describing gray-level and color images based on the associated Laguerre polynomials, which are orthogonal over the whole right-half plane. Moreover, the mathematical frameworks of radial associated Laguerre moments (RALMs) and associated rotation invariants are introduced. The proposed radial Laguerre invariants retain the basic form of disc-based moments, such as Zernike moments (ZMs), pseudo-Zernike moments (PZMs), Fourier-Mellin moments (OFMMs), and so on. Therefore, the rotation invariants of RALMs can be easily obtained. In addition, the study extends the proposed moments and invariants defined in a gray-level image to a color image using the algebra of quaternion to avoid losing some significant color information. Finally, the paper verifies the feature description capacities of the proposed moment function in terms of image reconstruction and invariant pattern recognition accuracy. Experimental results confirmed that the associated Laguerre moments (ALMs) perform better than orthogonal OFMMs in both noise-free and noisy conditions.

**Keywords:** *associated laguerre polynomials; orthogonal laguerre moments; quaternion; radial-polar; rotation invariants.*

## 1 Introduction

Orthogonal moment functions are one of the most important tools for the construction of shape descriptors for pattern recognition [1], object classification [2], template matching [3], image reconstruction [4], and data compression [5], etc. Among all kinds of moments, continuous ZMs, PZMs, OFMMs and Legendre moments were introduced by Teague and Teh, *et al.* in refs. [6]-[9] according to their corresponding polynomials as kernel functions. As is known to all, the computation of ZMs, PZMs and OFMMs requires the transformation from image coordinates to a region within the unit circle, and Legendre moments need to transform image coordinates into the interval  $[-1, 1]$ . In addition, discretization of the continuous integrals is necessary for the

computation of all continuous orthogonal moments. Discrete orthogonal moments provide a more accurate description for image features by evaluating moment components directly in the image coordinate space [10]-[13]. Hence, the discrete orthogonal moments eliminate the abovementioned problems associated with the continuous moments by using discrete orthogonal polynomials as kernel functions.

Recently, the problem of invariant pattern recognition which undergoes geometric transforms, such as rotation, scaling and translation (RST), has received increased interest in the pattern recognition field. Invariance feature selection always plays an important role in this subject. In recent decades, a number of orthogonal moments-based methods have been reported to construct an invariance feature [14]-[15]. Owing to the polar coordinate representation of the kernel functions of disc-based orthogonal moments, these continuous orthogonal moments have better image feature representation capabilities. This is mainly due to the fact that their rotation invariants can be easily constructed. Hence, as far as pattern recognition tasks is concerned, the continuous orthogonal moments still outperform discrete moments. Borrowing the specificity of the radial polynomials of disc-based moments, Mukundan [16] recently introduced the framework of radial Tchebichef moments, which is based on the structure of disc-based moments and is particularly suitable for pattern recognition works requiring rotation invariants.

In this paper, we propose another kind of discrete orthogonal moments, called associated Laguerre moments, which are also useful for image description. The proposed ALMs are defined in terms of the associated Laguerre polynomials [17], which are orthogonal over the whole right-half plane. The advantage of the proposed ALMs over disc-based continuous orthogonal moments lies in the fact that the computation of these continuous moments requires a coordinate transformation and suitable approximation of the integrals that are not existent in the proposed ALMs. Taking cues from Mukundan's research works [16], this study combines the merit of computational advantages of discrete orthogonal moments with shape description capabilities of continuous orthogonal moments, and introduces RALMs in polar-coordinate form. Thus, the shape descriptors of rotation invariants, which retain the basic form of disc-based continuous moments, can be easily constructed in terms of the magnitude of the proposed RALMs. Since the scale and translation invariance of a pattern can be achieved by other methods, such as Fourier methods [18], Mellin methods [19], Radon transform methods [20] and normalized methods [21] etc., this paper omits their discussion due to limited space. Furthermore, the proposed method obtains Q-ALMs and Q-RALMs by extending ALMs and RALMs to the quaternion field, and derives a set of rotation invariants based on them in order to deal with color images by using quaternion algebra. The advantage of this type of

representation is that a color image can be treated as a vector field. The accuracy of the proposed ALMs, RALMs, Q-ALMs, and Q-RALMs as global feature description capabilities is assessed by means of image reconstruction in noise-free and noisy cases and the results are compared with those of OFMMs. A classification experiment on gray-level and color images also illustrates the usefulness of the proposed feature descriptors.

The remainder of this paper is organized as follows: Section 2 gives some mathematical background on the associated Laguerre polynomials and quaternion algebra theory. Section 3 presents a set of discrete ALMs and RALMs, and investigates the rotational invariance of RALMs. In Section 4 presents the definition of Q-ALMs and Q-RALMs in a holistic manner. Section 5 presents the experimental results and illustrates the performance of the proposed shape descriptors, and Section 6 summarizes the paper.

## 2 Background

This section reviews the associated Laguerre polynomials and quaternion algebra, and presents some properties that will be useful in the rest of the paper.

### 2.1 Associated Laguerre Polynomials

It is well known that the associated Laguerre polynomials  $\{L_n^\alpha\}_{n \geq 0}$ , for  $\alpha > -1$ , are orthogonal with respect to the weight function  $w(x) = x^\alpha e^{-x}$  on the interval  $0 \leq x < +\infty$ , that is,

$$\int_0^\infty e^{-x} x^\alpha L_n^\alpha(x) L_m^\alpha(x) dx = \frac{\Gamma(n + \alpha + 1)}{n!} \delta_{nm}, \quad n, m \geq 0 \quad (1)$$

where  $\delta_{nm}$  is Kronecker's symbol. The associated Laguerre polynomials are defined as

$$L_n^\alpha(x) = \frac{(\alpha + 1)_n}{n!} {}_1F_1(-n; \alpha + 1; x) \quad (2)$$

where the Pochhammer symbol  $(\alpha)_k$  is as follows

$$(\alpha)_k = \alpha(\alpha + 1)(\alpha + 2) \dots (\alpha + k - 1) \quad \text{with } (\alpha)_0 = 1 \quad (3)$$

and  ${}_1F_1(-n; \alpha + 1; x)$  is a confluent hypergeometric function of the first kind

$${}_1F_1(a; b; z) = 1 + \frac{a}{b} z + \frac{a(a+1)}{b(b+1)} \frac{z^2}{2!} + \dots = \sum_{k=0}^{\infty} \frac{(a)_k}{(b)_k} \frac{z^k}{k!} \quad (4)$$

Together with Eqs. (4) and (2), the associated Laguerre polynomials can be rewritten as

$$L_n^\alpha(x) = \sum_{k=0}^n (-1)^k \frac{(n+\alpha)!}{(n-k)!(k+\alpha)!k!} x^k \quad (5)$$

The associated Laguerre polynomials satisfy the following second-order recurrence relation:

$$xL_n^{\alpha+1}(x) = (n+\alpha)L_{n-1}^\alpha(x) - (n-x)L_n^\alpha(x) \quad (6)$$

## 2.2 Quaternion Algebra

A quaternion has four components (one real part and three imaginary parts) and can be represented in a hyper-complex form as [22]

$$q = a + b \cdot i + c \cdot j + d \cdot k \quad (7)$$

where  $a, b, c, d \in \mathbb{R}$ , and  $i, j, k$  obey the following multiplication rules:

$$\begin{aligned} i^2 = j^2 = k^2 = -1, i \times j = -j \times i = k, \\ j \times k = -k \times j = i, k \times i = -i \times k = j \end{aligned} \quad (8)$$

The modulus of a quaternion  $q$  follows the definition for complex numbers as

$$|q| = \sqrt{a^2 + b^2 + c^2 + d^2} \quad (9)$$

It is often useful to consider a quaternion as the sum of a scalar part and a vector part, which is represented as

$$q = S(q) + V(q) \quad (10)$$

where  $S(q) = a$  and  $V(q) = b \cdot i + c \cdot j + d \cdot k$ . If  $S(q) = 0$ , then  $q$  is reduced to a pure quaternion.

## 2.3 Associated Laguerre Moments

Without loss of generality, the ALMs of an image  $f(x, y)$  with order of  $m+n$  and size of  $N \times N$  are defined by the normalized associated Laguerre orthogonal polynomials  $\tilde{L}_n^\alpha(x)$  as follows

$$\tilde{S}_{mn}^\alpha = \sum_{x=0}^{N-1} \sum_{y=0}^{N-1} \tilde{L}_m^\alpha(x) \tilde{L}_n^\alpha(y) f(x, y), \quad m, n = 0, 1, \dots, N-1. \quad (11)$$

Considering the set of associate Laguerre polynomials,  $\{L_n^{(\alpha)}\}_{n \geq 0}$  is not suitable for defining moments because the range of values of the polynomials expands rapidly with the increase of order. To avoid numerical fluctuation in the moment computation, the current study applies normalized associated orthogonal Laguerre polynomials  $\tilde{L}_n^\alpha(x)$  to define the proposed ALMs.

$$\tilde{L}_n^\alpha(x) = \sqrt{\frac{x^\alpha e^{-x} n!}{(n+k)!}} L_n^\alpha(x) \quad (12)$$

The first few orders of the normalized associated Laguerre polynomials with the parameters  $\alpha = 0, 1, 2$  are shown in Figure 1. From Figure 1 one can observe clearly that the values of normalized associated polynomials  $\tilde{L}_n^\alpha(x)$  are bounded on a finite interval and have a notable difference from the associated polynomials  $L_n^\alpha(x)$ .

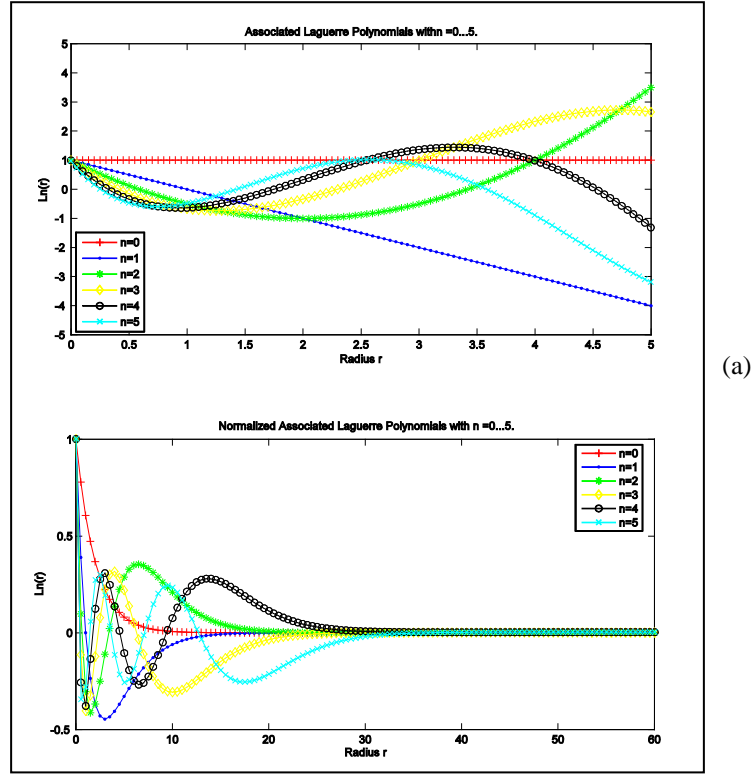
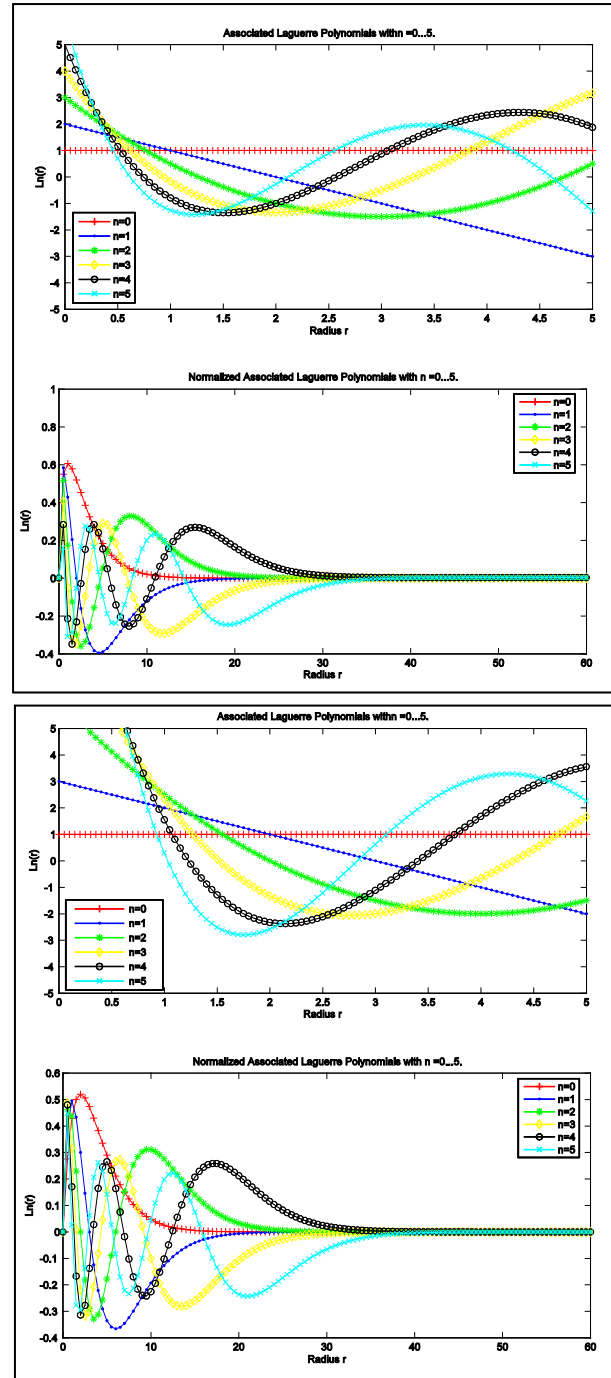


**Figure 1** Plot the  $L_n^\alpha(x)$  and  $\tilde{L}_n^\alpha(x)$ , (a)  $\alpha = 0$ ; (b)  $\alpha = 1$ ; (c)  $\alpha = 2$ .



(b)

(c)

**Figure 1** *Continued.* Plot the  $L_n^\alpha(x)$  and  $\tilde{L}_n^\alpha(x)$ , (a)  $\alpha = 0$ ; (b)  $\alpha = 1$ ; (c)  $\alpha = 2$ .

Comparing Eq. (1) and Eq. (12), one can obtain the orthogonality condition of normalized associated polynomials  $\tilde{L}_n^\alpha(x)$  as

$$\int_0^\infty \tilde{L}_n^\alpha(x) \tilde{L}_m^\alpha(x) dx = \delta_{nm}, \quad n, m \geq 0 \quad (13)$$

The performance of moment descriptor  $\tilde{S}_{mn}^\alpha$  is well assessed by means of image reconstruction. Thanks to the orthogonality and completeness of  $\{\tilde{L}_n^\alpha(x)\}$ , which allow one to represent any square integrable image  $f(x, y)$  via a truncated series defined over whole right-half plane, to be written by

$$\hat{f}(x, y) = \sum_{m=0}^{N-1} \sum_{n=0}^{N-1} \tilde{S}_{mn}^\alpha \tilde{L}_m^\alpha(x) \tilde{L}_n^\alpha(y) \quad (14)$$

It should be expected that the representation in the above formula can converge to the true image by making orders  $N$  sufficiently large.

## 2.4 Radial associated Laguerre Moments

Rotational invariance is an inherent property of disc-based continuous orthogonal moments. However, as indicated in Eq. (11), the proposed ALMs are defined over the Cartesian coordinates, therefore, it is still not convenient enough to generate rotation invariants. Motivated and aided by the framework of Zernike radial polynomials, this study therefore tries to define the following RALMs of order  $p$  and repetition  $q$  as

$$\tilde{R}_{pq}^\alpha = \frac{1}{2\pi} \sum_{r=0}^{m-1} \sum_{\theta=0}^{2\pi} \tilde{L}_p^\alpha(r) e^{-jq\theta} f(r, \theta) \quad (15)$$

where the image has a size of  $N \times N$  pixels and  $m$  denotes  $N/2$ . Since  $\theta$  is a real quantity measured in radians, one can rewrite (15) as

$$\tilde{R}_{pq}^\alpha = \frac{1}{n} \sum_{r=0}^{m-1} \sum_{\theta=0}^{n-1} \tilde{L}_p^\alpha(r) e^{-jq\theta} f(r, \theta) \quad (16)$$

where  $n$  is at 360. When the image is sampled at one-degree intervals and the coordinates  $x, y$  are given by

$$x = \frac{rN}{2(m-1)} \cos\left(\frac{2\pi\theta}{n}\right) + \frac{N}{2}, \quad y = \frac{rN}{2(m-1)} \sin\left(\frac{2\pi\theta}{n}\right) + \frac{N}{2} \quad (17)$$

the structure of the RALMs is very similar to that of disc-based moments. It can also be easily found that the definition in Eq. (16) yields a set of moments that is orthogonal in the discrete polar coordinate space of the image. Moreover, the main purpose of this type of representation is that the rotation invariants can be

easily derived. Given an image  $f(r, \theta)$ , after rotation by an angle  $\alpha$ , the image is  $f(r, \theta + \phi)$ . One has

$$\begin{aligned}\hat{R}_{pq}^\alpha &= \frac{1}{2\pi} \int_0^1 \int_0^{2\pi} r \tilde{L}_p^\alpha(r) f(r, \theta + \phi) e^{-jq(\theta + \phi)} dr d\theta \\ &= e^{-jq\phi} \frac{1}{2\pi} \int_0^1 \int_0^{2\pi} r \tilde{L}_p^\alpha(r) f(r, \theta) e^{-jq\theta} dr d\theta \\ &= e^{-jq\phi} \tilde{R}_{pq}^\alpha\end{aligned}\quad (18)$$

After applying normal operations, we have

$$\hat{R}_{pq}^\phi = e^{-jq\phi} \tilde{R}_{pq}^\alpha = \|e^{-jq\phi}\| \cdot \|\tilde{R}_{pq}^\alpha\| = \|\tilde{R}_{pq}^\alpha\| \quad (19)$$

Comparing Eq. (18) with Eq. (19), it is not difficult to see that  $\|\tilde{R}_{pq}^\alpha\|$  is with rotational invariance. The corresponding inverse moments transform is given by the following equation:

$$\hat{f}(r, \theta) = \sum_{p=0}^P \sum_{q=0}^Q \tilde{R}_{pq}^\alpha \tilde{L}_p^\alpha(r) e^{jq\theta} \quad (20)$$

### 3 Quaternion associated Laguerre Moments

Let  $f(r, \theta) \equiv f_R i + f_G j + f_B k = f_R(r, \theta) i + f_G(r, \theta) j + f_B(r, \theta) k$  be an RGB image defined in polar coordinates. Therefore, the forward Q-ALMs can be defined as

$$\begin{aligned}\widetilde{QS}_{mn}^\alpha &= \sum_{x=0}^{N-1} \sum_{y=0}^{N-1} \tilde{L}_m^\alpha(x) \tilde{L}_n^\alpha(y) (if_R + jf_G + kf_B) \mu \\ &= -\frac{1}{\sqrt{3}} \sum_{x=0}^{N-1} \sum_{y=0}^{N-1} \tilde{L}_m^\alpha(x) \tilde{L}_n^\alpha(y) (if_R + jf_G + kf_B) (i + j + k) \\ &= -\frac{1}{\sqrt{3}} \left[ \sum_{x=0}^{N-1} \sum_{y=0}^{N-1} \tilde{L}_m^\alpha(x) \tilde{L}_n^\alpha(y) (f_R + f_G + f_B) \right] \\ &\quad - \frac{1}{\sqrt{3}} i \left[ \sum_{x=0}^{N-1} \sum_{y=0}^{N-1} \tilde{L}_m^\alpha(x) \tilde{L}_n^\alpha(y) (f_G - f_B) \right] \\ &\quad - \frac{1}{\sqrt{3}} j \left[ \sum_{x=0}^{N-1} \sum_{y=0}^{N-1} \tilde{L}_m^\alpha(x) \tilde{L}_n^\alpha(y) (f_B - f_R) \right] \\ &\quad - \frac{1}{\sqrt{3}} k \left[ \sum_{x=0}^{N-1} \sum_{y=0}^{N-1} \tilde{L}_m^\alpha(x) \tilde{L}_n^\alpha(y) (f_R - f_G) \right]\end{aligned}\quad (21)$$

where  $\mu$  is a unit pure quaternion chosen as  $\mu = (i + j + k) / \sqrt{3}$  in the current study. Thus, Eq. (21) can be rewritten as

$$\widetilde{QS}_{mn}^{\alpha} = A_0^R + iA_1^R + jA_2^R + kA_3^R \quad (22)$$

where

$$\begin{aligned} A_0^R &= \frac{1}{\sqrt{3}} [\tilde{S}_{mn}^{\alpha}(f_R) + \tilde{S}_{mn}^{\alpha}(f_G) + \tilde{S}_{mn}^{\alpha}(f_B)] \\ A_1^R &= -\frac{1}{\sqrt{3}} [\tilde{S}_{mn}^{\alpha}(f_G) - \tilde{S}_{mn}^{\alpha}(f_B)] \\ A_2^R &= -\frac{1}{\sqrt{3}} [\tilde{S}_{mn}^{\alpha}(f_B) - \tilde{S}_{mn}^{\alpha}(f_R)] \\ A_3^R &= -\frac{1}{\sqrt{3}} [\tilde{S}_{mn}^{\alpha}(f_R) - \tilde{S}_{mn}^{\alpha}(f_G)] \end{aligned} \quad (23)$$

As discussed in the above section, since the associated Laguerre polynomials are orthogonal, color images can be estimated from a finite number  $N$  of Q-ALMs using the following inverse moment transform:

$$\begin{aligned} \hat{f}(x, y) &= \sum_{m=0}^{N-1} \sum_{n=0}^{N-1} \widetilde{QS}_{mn}^{\alpha} \tilde{L}_m^{\alpha}(x) \tilde{L}_n^{\alpha}(y) \mu \\ &= -\frac{1}{\sqrt{3}} \sum_{m=0}^{N-1} \sum_{n=0}^{N-1} (A_0^R + iA_1^R + jA_2^R + kA_3^R) \tilde{L}_m^{\alpha}(x) \tilde{L}_n^{\alpha}(y) (i + j + k) \\ &= -\frac{1}{\sqrt{3}} \left[ \sum_{m=0}^{N-1} \sum_{n=0}^{N-1} \tilde{L}_m^{\alpha}(x) \tilde{L}_n^{\alpha}(y) (A_1^R + A_2^R + A_3^R) \right] \\ &\quad - \frac{1}{\sqrt{3}} i \left[ \sum_{m=0}^{N-1} \sum_{n=0}^{N-1} \tilde{L}_m^{\alpha}(x) \tilde{L}_n^{\alpha}(y) (A_0^R + A_2^R - A_3^R) \right] \\ &\quad - \frac{1}{\sqrt{3}} j \left[ \sum_{m=0}^{N-1} \sum_{n=0}^{N-1} \tilde{L}_m^{\alpha}(x) \tilde{L}_n^{\alpha}(y) (A_0^R - A_1^R + A_3^R) \right] \\ &\quad - \frac{1}{\sqrt{3}} k \left[ \sum_{m=0}^{N-1} \sum_{n=0}^{N-1} \tilde{L}_m^{\alpha}(x) \tilde{L}_n^{\alpha}(y) (A_0^R + A_1^R - A_2^R) \right] \end{aligned} \quad (24)$$

The right-side Q-RALMs of order  $p$  with repetition  $q$  are defined as follows

$$\begin{aligned}
\widetilde{Q}R_{pq}^\alpha &= \frac{1}{2\pi} \int_0^1 \int_0^{2\pi} r \tilde{L}_p^\alpha(r) f(r, \theta) e^{-\mu q \theta} dr d\theta \\
&= \frac{1}{2\pi} \int_0^1 \int_0^{2\pi} r \tilde{L}_p^\alpha(r) (f_R i + f_G j + f_B k) (\cos(-q\theta) + \mu \sin(-q\theta)) dr d\theta \\
&= \left( \text{Re}(\tilde{R}_{pq}^\alpha(f_R)) + \mu \text{Im}(\tilde{R}_{pq}^\alpha(f_R)) \right) i + \left( \text{Re}(\tilde{R}_{pq}^\alpha(f_G)) + \mu \text{Im}(\tilde{R}_{pq}^\alpha(f_G)) \right) j \\
&\quad + \left( \text{Re}(\tilde{R}_{pq}^\alpha(f_B)) + \mu \text{Im}(\tilde{R}_{pq}^\alpha(f_B)) \right) k \\
&= -\frac{1}{\sqrt{3}} \left( \text{Im}(\tilde{R}_{pq}^\alpha(f_R)) + \text{Im}(\tilde{R}_{pq}^\alpha(f_G)) + \text{Im}(\tilde{R}_{pq}^\alpha(f_B)) \right) \\
&\quad + \left\{ \text{Re}(\tilde{R}_{pq}^\alpha(f_R)) + \frac{1}{\sqrt{3}} \left[ \text{Im}(\tilde{R}_{pq}^\alpha(f_G)) - \text{Im}(\tilde{R}_{pq}^\alpha(f_B)) \right] \right\} i \\
&\quad + \left\{ \text{Re}(\tilde{R}_{pq}^\alpha(f_G)) + \frac{1}{\sqrt{3}} \left[ \text{Im}(\tilde{R}_{pq}^\alpha(f_B)) - \text{Im}(\tilde{R}_{pq}^\alpha(f_R)) \right] \right\} j \\
&\quad + \left\{ \text{Re}(\tilde{R}_{pq}^\alpha(f_B)) + \frac{1}{\sqrt{3}} \left[ \text{Im}(\tilde{R}_{pq}^\alpha(f_R)) - \text{Im}(\tilde{R}_{pq}^\alpha(f_G)) \right] \right\} k
\end{aligned} \tag{25}$$

From such a representation, the rotation invariants are easily achieved by taking the modulus of Q-RALMs. Similar approaches can be used to obtain left-side Q-RALMs. Owing to limited space we will omit their discussion.

#### 4 Experimental Results

Several experiments were carried out to evaluate the performance of the proposed ALMs and RALMs. The experiments used six selected test images (shown in Figure 2), including gray-level images and color images, with a resolution of 256×256 and 128×128, respectively.

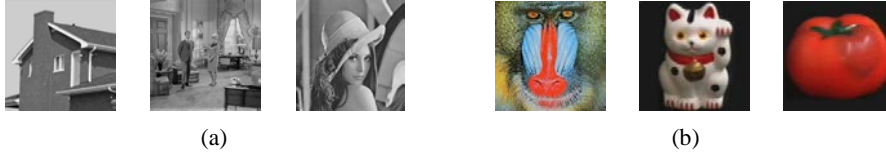


**Figure 2** Original test images, (a) gray-level images (size: 256×256); (b) color images (size: 128×128).

The mean square error (MSE) was used as the fidelity criteria measuring the resemblance between the reconstructed images and the original ones. It can be written as

$$\varepsilon = \frac{\|f(x, y) - \hat{f}(x, y)\|^2}{\|f(x, y)\|^2} \quad (26)$$

where  $\|\cdot\|$  is the standard Euclidean norm,  $f(x, y)$  and  $\hat{f}(x, y)$  respectively represent the original test and the reconstructed image.

#### 4.1 Image Reconstruction

The most effective method to test image description capability of moment functions is by image reconstruction. By virtue of orthogonal function theory shown in Eq. (13), both gray-level and color images can be estimated approximately by Eq. (14). Figure 3 shows the reconstruction result using ALMs and Q-ALMs for various values of the parameter  $\alpha$ . The second experiment was carried out to illustrate the image discrimination power of the RALMs using a Chinese character with a size of  $64 \times 64$  pixels, as listed in Table 1. The reconstruction results were compared with those using orthogonal OFMMs. This analysis was repeated with a gray-level image with a size of  $128 \times 128$  pixels, as shown in Figure 4. From Table 1 and Figure 4 we can find that the reconstruction based on ALMs outperformed the other two types of orthogonal moments. It is observed that the reconstructed images using OFMMs exhibited a peculiar behavior in the vicinity of the image center. This phenomenon was more prominent for very high orders of moments.

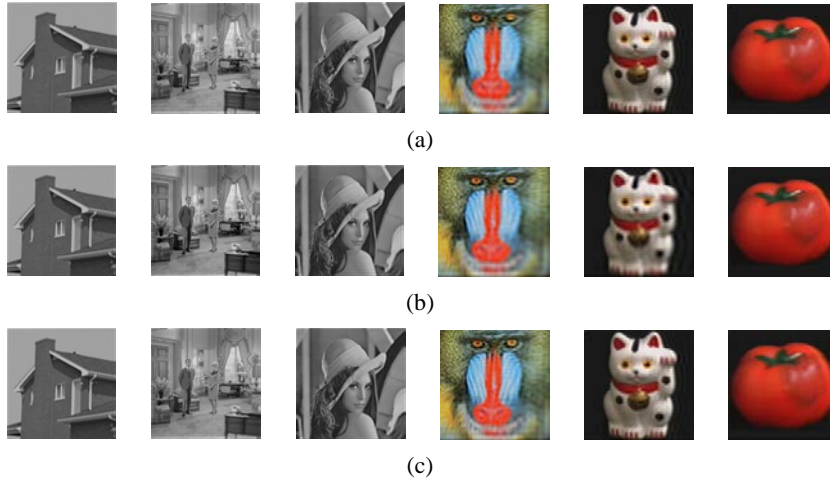


**Figure 3** Reconstructed images using ALMs and Q-ALMs for gray-level images and color images, respectively, (a)  $\alpha = 0$ ; (b)  $\alpha = 1$ ; (c)  $\alpha = 2$ .

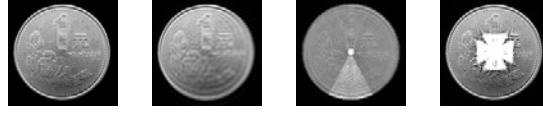
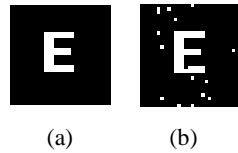


**Figure 4** Reconstruction of gray-level image using ALMs ( $\alpha = 2$ ), RALMs ( $\alpha = 2$ ) and OFMMs; (a) origin image; (b) ALMs; (c) RALMs; (d) OFMMs.

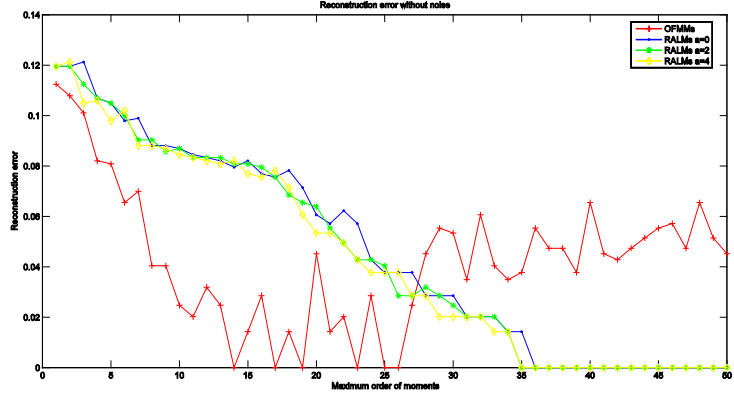
**Table 1** Reconstruction using RALMs with different  $m$ ,  $n$ ,  $P$ ,  $Q$ .

Image	Reconstruction Parameter
	Original image with size $N = 64$
	RALMs methods ( $\alpha = 2$ ) $m = 32, n = 384, P_{\max} = 30, Q_{\max} = 100, \varepsilon = 272$
	RALMs methods ( $\alpha = 2$ ) $m = 32, n = 384, P_{\max} = 64, Q_{\max} = 300, \varepsilon = 44$
	ALMs methods ( $\alpha = 2$ ) $P_{\max} = 64, \varepsilon = 32$
	OFMMs methods $P_{\max} = 64, \varepsilon = 39$

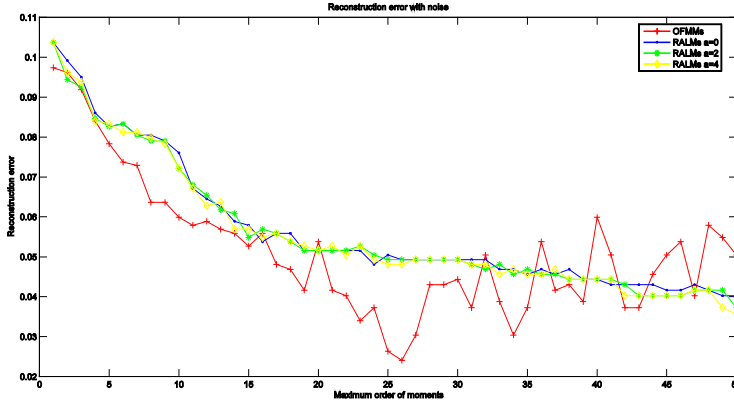
It is well known that noise may severely affect the quality of image reconstruction. To evaluate the robustness of moments with regards to different kinds of noises, we tested the noise robustness of different orthogonal moments. Pepper-and-salt noise at 5% was added to the original binary image ‘E’ (see Figure 5). Figure 6 shows the reconstruction results using different orthogonal moments, and the corresponding mean square error comparison is depicted in Figure 6(b). Figures 6(a) and (b) show that the reconstruction error of the English letter ‘E’ using RALMs was a little smaller than using other methods with the increase of order.



**Figure 5** The English letter ‘E’, (a) letter ‘E’ without noise; (b) letter ‘E’ with 5% salt-and-pepper noise.



(a)



(b)

**Figure 6** Reconstruction error, (a) noise-free case; (b) salt-and-pepper noise case (5%).

## 4.2 Rotation Invariant Recognition

This subsection reports a detailed experimental study on the recognition accuracy of RALMs in both noise-free and noisy cases for binary images, gray-level images, and color images, respectively. According to the definition of RALMs, we can easily know that the magnitude of RALMs remains invariant under image rotation. Thus, they are useful features for rotation-invariant pattern recognition. In the current recognition task, the following feature vectors of rotational invariance were chosen

$$V = [\|\tilde{R}_{21}^{\alpha}\|, \|\tilde{R}_{32}^{\alpha}\|, \|\tilde{R}_{33}^{\alpha}\|, \|\tilde{R}_{41}^{\alpha}\|, \|\tilde{R}_{42}^{\alpha}\|, \|\tilde{R}_{43}^{\alpha}\|, \|\tilde{R}_{44}^{\alpha}\|] \quad (27)$$

The Euclidean distance was utilized as the classification measure

$$d(V_s, V_t^{(k)}) = \sum_{j=1}^T (v_{sj} - v_{tj}^{(k)})^2 \quad (28)$$

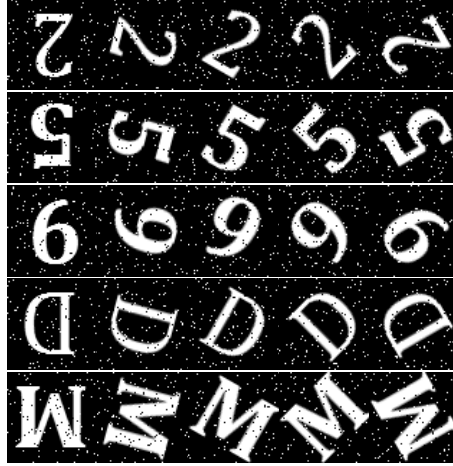
where  $V_s$  is the  $T$ -dimensional feature vector for the unknown sample and  $V_t^{(k)}$  is the training vector for class  $k$ . We defined the recognition accuracy  $\eta$  as

$$\eta = \frac{\text{Number of correctly classified images}}{\text{The total number of image used in the test}} 100\% \quad (29)$$

The classification experiment was carried out to test the performance of RALM rotation moments invariants. A set of similar binary characters with sizes of  $64 \times 64$  pixels, shown in Figure 7, was used as the training set. The experiment was done for such a character set since elements in this set can be easily misclassified owing to their similarity. Each testing set consisted of 720 images, which were generated by rotating the training images to every 5 degrees in the range of  $[0, 360)$ . Then, each image in the training set was degraded by 5% pepper-and-salt noise. Figure 8 shows part of these testing images. The experiments were repeated for each parameter  $\alpha$ . Table 2 shows the classification results using different moment invariants. As can be observed from this table, RALMs achieved higher recognition rates.



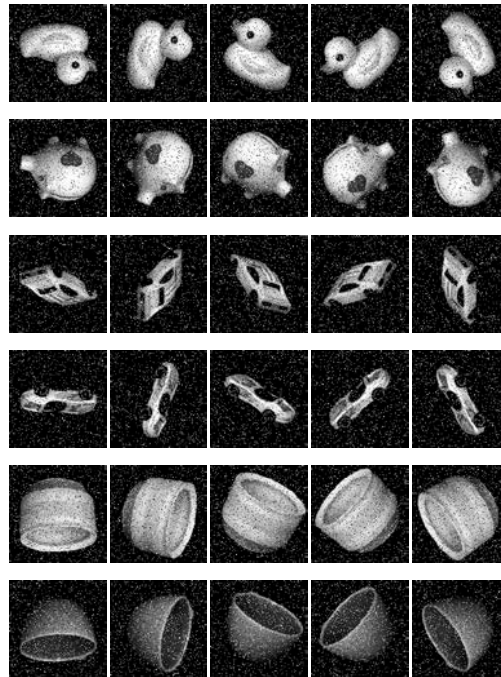
**Figure 7** Part of binary characters training set.



**Figure 8** Part of binary characters testing set with 5% pepper-and-salt noise.

**Table 2** Classification results comparison with different salt-and-pepper noises.

Method	Parameter $a$	Noise-free	5%	8%	10%	15%	20%
RALMs	0	80%	72%	74%	64%	52%	56%
	2	100%	100%	94%	92%	76%	66%
	4	100%	92%	78%	74%	66%	60%
	6	100%	84%	70%	68%	52%	48%
	8	100%	84%	66%	66%	54%	46%
	10	100%	66%	56%	52%	48%	42%
	15	100%	98%	92%	84%	76%	54%
	20	100%	86%	66%	50%	40%	26%
OFMMs		100%	86%	78%	72%	60%	62%

**Figure 9** Part of gray-level objects training set.**Figure 10** Part of gray-level objects testing set with 10% pepper-and-salt noise.

To illustrate the discrimination power of RALMs for noisy gray-level images several gray-level training images with a size of  $128 \times 128$  pixels from the Columbia object image database [23] were chosen (shown in Figure 9). A new set of 720 images was generated as the testing set by rotating the training images from  $0^\circ$  to  $360^\circ$  with an interval of  $5^\circ$ . This was followed by adding salt-and-pepper noise with different noise densities, as shown in Figure 10. In the classification work, seven invariants of RALMs and OFMMs were calculated and the Euclidean distance was used here as the classification measure. The results of the classification are depicted in Table 3 and one can observe from this table that RALMs achieved higher recognition rates in the noise case.

**Table 3** Classification results comparison with different salt-and-pepper noises.

Method	Parameter $\alpha$	Noise-free	5%	8%	10%	15%	20%
RALMs	0	96%	88%	66%	62%	62%	44%
	2	100%	96%	92%	88%	74%	66%
	4	100%	98%	92%	94%	78%	76%
	6	100%	98%	96%	98%	86%	80%
	8	100%	100%	96%	98%	80%	84%
	10	100%	100%	100%	100%	80%	72%
	15	100%	80%	80%	78%	78%	72%
	20	100%	100%	94%	86%	60%	50%
OFMMs		100%	100%	100%	88%	84%	74%

The final experiment was aimed at finding out how well the proposed invariants perform for color image recognition. Color images were generated from the same image dataset as the training set [23]. They were cropped and rotated to a standard size of  $128 \times 128$  pixels. Some samples of these training images are given in Figure 11. The testing images were generated from the training images by rotating them with rotation angle  $\theta = 5, 10, 15, \dots, 360^\circ$  and then contaminating them with pepper-and-salt noise with a density of 20% (see Figure 12). In order to investigate the role of the parameter  $\alpha$  in the recognition performance, the experiments were repeated for each parameter  $\alpha$ . The classification rates for the OFMMs-based method and Q-RALMs method are given in Table 4. It was clearly found that the Q-RALMs had a better classification performance at parameter  $\alpha = 6, 8, 10$ .



**Figure 11** Part of color images training set.

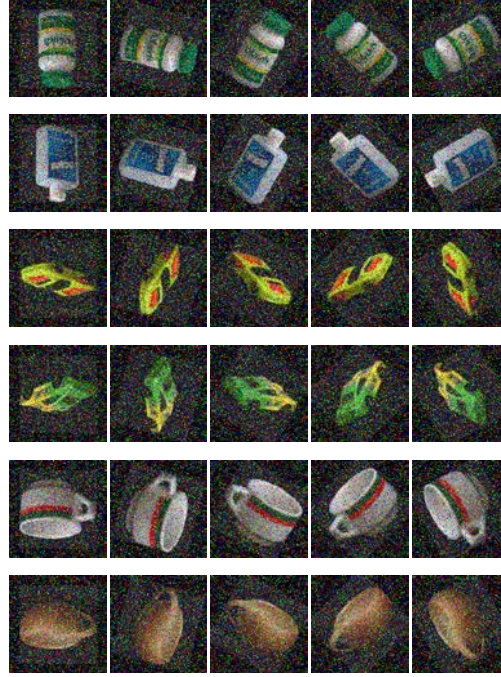


**Figure 12** Part of color images testing set with 20% pepper-and-salt noise.

**Table 4** Classification results comparison with different salt-and-pepper noises.

Method	Parameter $\alpha$	Noise-free	5%	8%	10%	15%	20%
RALMs	0	80%	66%	68%	56%	48%	40%
	2	100%	94%	82%	74%	74%	62%
	4	100%	88%	88%	80%	78%	66%
	6	100%	94%	94%	84%	66%	68%
	8	100%	100%	100%	98%	90%	80%
	10	100%	100%	100%	98%	90%	78%
	15	100%	84%	78%	76%	68%	62%
	20	100%	98%	94%	88%	76%	62%
OFMMs		100%	100%	96%	94%	84%	64%

All above the experiments indicated that the parameter  $\alpha$  plays an important role in the pattern recognition task when using the invariants of the RALMs-based method, as it controls the shifting to the image region of interest. The choice of the parameter  $\alpha$  corresponding to the case where the emphasis of the moments is at the center of the image gave the best reconstruction result. The classification

experiment demonstrated that the best recognition accuracy was achieved for  $\alpha$  from 6 to 10 under both noise-free and noisy conditions.

## 5 Conclusions

This paper introduced a new type of orthogonal moments based on the associated Laguerre polynomials for image description, and constructed RALMs using methods that are similar to those of disc-based moments. This form makes them particularly suitable for pattern recognition tasks requiring rotation invariants. In addition, the study extended the proposed moments and rotation invariants defined for gray-level images to color images using the theory of quaternion algebra. The numerical experiment results obtained from both gray-level images and color images demonstrate that the effectiveness of the proposed ALMs and RALMs could be better according to description performance and invariant pattern recognition capabilities in noise-free and noisy cases.

## References

- [1] Zhang, H., Shu, H., Han, G.N., Coatrieux, G., Luo, L. & Coatrieux, J.L., *Blurred Image Recognition by Legendre Moment Invariants*, IEEE Transactions on Image Processing, **19**(3), pp. 596-611, 2010.
- [2] Jain, S., Papadakis, M., Upadhyay, S. & Azencott, R., *Rigid-motion-invariant Classification of 3-D Textures*, IEEE Transactions on Image Processing, **21**(5), pp. 2449-2463, 2012.
- [3] Lin, Y.H. & Chen, C.H., *Template Matching Using the Parametric Template Vector with Translation, Rotation and Scale Invariance*, Pattern Recognit., **41**(7), pp. 2413-2421, 2008.
- [4] Yap, P.-T., Jiang, X. & Kot, A.C., *Two-Dimensional Polar Harmonic Transforms for Invariant Image Representation*, IEEE Trans. Pattern Anal. & Mach. Intell., **32**(7), pp. 1259-1270, 2010.
- [5] See, K.W., Loke, K.S., Lee, P.A. & Loe, K.F., *Image Reconstruction Using Various Discrete Orthogonal Polynomials in Comparison with DCT*, Applied Mathematics and Computation, **193**(2), pp. 346-359, 2007.
- [6] Teh, C.H. & Chin, R.T., *On Image Analysis by the Methods of Moments*, IEEE Transactions on Pattern Analysis and Machine Intelligence, **10**(4), pp. 496-513, 1988.
- [7] Teague, M.R., *Image Analysis via the General Theory of Moments*, Journal of the Optical Society of America, **70**(8), pp. 920-930, 1980.
- [8] Mukundan, R. & Ramakrishnan, K.R., *Moment Functions in Image Analysis-Theory and Applications*, World Scientific, Singapore, 1998.

- [9] Sheng, Y. & Arsenault, H.H., *Experiments on Pattern Recognition Using Invariant Fourier-Mellin Descriptors*, J. Opt. Soc. Am. A, **3**(6), pp. 771-776, 1986.
- [10] Mukundan, R., Ong, S.H. & Lee, P.A., *Image Analysis by Tchebichef Moments*, IEEE Transactions on Image Processing, **10**(9), pp. 1357-1364, 2001.
- [11] Yap, P.T., Paramesran, R. & Ong, S.H., *Image Analysis by Krawtchouk Moments*, IEEE Transactions on Image Processing, **12**(11), pp. 1367-1377, 2003.
- [12] Zhu, H.Q. Shu, H.Z., Liang, J., Luo, L.M. & Coatrieux, J.L. *Image Analysis by Discrete Orthogonal Racah Moments*, Signal Processing **87**(4), pp. 687-708, 2007.
- [13] Zhu, H.Q., Shu, H.Z., Zhou, J., Luo, L.M. & Coatrieux, J.L., *Image Analysis by Discrete Orthogonal Dual Hahn Moments*, Pattern Recognition Letters, **28**(13), pp. 1688-1704, 2007.
- [14] Chen, B., Shu, H., Zhang, H., Coatrieux, G., Luo, L. & Coatrieux, J. L. *Combined Invariants to Similarity Transformation and to Blur Using Orthogonal Zernike Moments*, IEEE Trans. Image Process., **20**(2), pp. 345-360, 2011.
- [15] Yang, B. & Dai, M., *Image Analysis by Gaussian-Hermite Moments*, Signal Processing, **91**(10), pp. 2290-2303, 2011.
- [16] Mukundan, R., *A New Class of Rotation Invariants Using Discrete Orthogonal Moments*, Honolulu, USA: Proceedings of the 6<sup>th</sup> IASTED International Conference, Signal and Image Processing, 2004.
- [17] Askey, R. & Wimp, J., *Associated Laguerre and Hermite Polynomials*, Proc. Roy. Soc. Edinburgh Sect. A., **96**(1-2), pp. 15-37, 1984.
- [18] Howell, K.B., *Fourier Transforms, in Transforms and Applications Handbook*, 3<sup>rd</sup> ed., A. D. Poularikas, Ed., ch.2, CRC Press, Boca Raton, FL, U.S.A, 2010.
- [19] Xiao, B., Ma, J.-F. & Cui, J.-T., *Combined Blur, Translation, Scale and Rotation Invariant Image Recognition by Radon and Pseudo-Fourier-Mellin Transforms*, Pattern Recognition, **45**(1), pp. 314-321, 2012.
- [20] Zhu, H., Liu, M. & Li, Y. *The RST Invariant Digital Image Watermarking Using Radon Transforms and Complex Moments*, Digital Signal Processing, **20**(6), pp. 1612-1628, 2010
- [21] Nasir, I., Khelifi, F. Jiang, J. & Ipson, S., *Robust Image Watermarking via Geometrically Invariant Feature Points and Image Normalization*, IET Image Process., **6**(4), pp. 354-363, 2012.
- [22] Hamilton, W.R., *Elements of Quaternions*, London, U.K.: Longmans, Green, 1866.
- [23] <http://www1.cs.columbia.edu/CAVE/software/softlib/coil-20.php> (24 May 2013).